

Niğde Ömer Halisdemir Üniversitesi Mühendislik Bilimleri Dergisi Niğde Ömer Halisdemir University Journal of Engineering Sciences

Araştırma makalesi / Research article

www.dergipark.org.tr/tr/pub/ngumuh / www.dergipark.org.tr/en/pub/ngumuh



Investigation of the effects of heavy and light welding on buckling behavior of square hollow sections: Parametric study

Ağır ve hafif kaynak işlemlerinin kare kesitli boş profillerin burkulma davranışı üzerindeki etkilerinin incelenmesi: Parametrik bir çalışma

Osman Özenç^{1,*} , Mehmet Akif Dündar²

^{1,2} Yozgat Bozok Universty, Faculty of Engineering and Architecture, Mechanical Engineering Department, 66100, Yozgat, Türkiye

Abstract

This parametric study examines the influence of residual stresses from light and heavy welding on the local elastic buckling behavior of square hollow sections (SHSs) with welded corners, under axial compression and major axis bending. By analyzing various SHS sizes with a constant height-to-thickness ratio of 40, this investigation provides insights into how residual stress levels impact load-bearing capacity. Findings reveal a pronounced impact of heavy welding-induced residual stresses, notably diminishing the critical buckling loads across both loading conditions. Specifically, under axial compression, heavy welding led to a significant reduction in bifurcation loads approximately 15.3%, while light welding caused a reduction of around 7.5%. In major axis bending, the effects were similarly considerable, with bifurcation moments reduced by approximately 12.78% for heavy welding and by 6.16% for light welding. The findings underscore the substantial effect of residual stress, particularly from heavy welding, on axial compression, indicating a greater sensitivity of SHSs to this loading condition relative to major axis bending. This study emphasizes the need for careful consideration of welding type in design practices to ensure structural reliability.

Keywords: Square Hollow Sections (SHSs), Local elastic buckling residual stress, Heavy and light welding, Finite element analysis

1 Introduction

Square hollow sections (SHSs) play a critical role in modern structural engineering and construction, valued for their geometric efficiency and aesthetic appeal. Renowned for their exceptional strength, adaptability, and ease of fabrication, SHSs are integral to contemporary engineering applications [1–3]. The closed cross-sectional configuration of SHSs provides notable advantages over open sections, such as improved torsional resistance, enhanced structural stability, and more uniform stress distribution [4–7]. These characteristics render SHSs highly suitable for applications demanding high load-bearing capacity and rigidity, including building frameworks, bridges, and other

Öz

Bu parametrik çalışma, eksenel basınç ve ana eksen eğilmesi altında, kaynaklı köşelere sahip kare kesitli boş profillerin (SHS) yerel elastik burkulma davranışı üzerindeki hafif ve ağır kaynak işleminden kaynaklanan artık gerilmelerin etkisini incelemektedir. Sabit bir yükseklik-et kalınlığı oranı (40) ile çeşitli SHS boyutlarının analizi yoluyla, artık gerilme seviyelerinin yük taşıma kapasitesi üzerindeki etkileri hakkında önemli bulgular sunulmaktadır. Bulgular, ağır kaynak işlemiyle oluşan artık gerilmelerin kritik burkulma yüklerini her iki yükleme durumunda da belirgin bir şekilde azalttığını ortaya koymaktadır. Özellikle, eksenel basınç altında ağır kaynak, yaklaşık %15.3 oranında çatallanma yüklerinde önemli bir azalmaya yol açarken, hafif kaynak ise yaklaşık %7.5 oranında bir azalma sağlamıştır. Ana eksen eğilmesi durumunda da benzer şekilde önemli etkiler gözlemlenmiş olup, çatallanma momentleri ağır kaynak için yaklaşık %12.78, hafif kaynak için ise %6.16 oranında azalmıştır. Bulgular, özellikle ağır kaynaktan kaynaklanan artık gerilmenin eksenel basınç üzerindeki önemli etkisini vurgulamakta ve SHS'lerin bu yükleme koşuluna, ana eksen eğilmesine kıyasla daha hassas olduğunu göstermektedir. Bu çalışma, yapısal güvenilirliği sağlamak için tasarım uygulamalarında kaynak türünün dikkatlice değerlendirilmesi gerektiğini vurgulamaktadır.

Anahtar Kelimeler: Kare Kesitli Boş Profiller, Yerel elastik burkulma, Artık gerilme, Ağır ve hafif kaynak, Sonlu elemanlar analizi

infrastructure projects [8, 9]. The versatility and durability of SHSs ensure their continued importance in the design and implementation of advanced engineering solutions [10,11]. In such applications, the design of SHSs is crucial to prevent structural failures and maintain safety. Optimizing design and performing rigorous stress analysis not only enhance structural performance and longevity but also mitigate risks and ensure compliance with stringent engineering standards [12–15]. Due to their thin-walled construction, however, SHSs are particularly susceptible to global buckling, local elastic buckling, and post-buckling, indicating that strength alone is insufficient for robust design [12]. Addressing these buckling phenomena through comprehensive design

^{*} Sorumlu yazar / Corresponding author, e-posta / e-mail: : osman.ozenc@yobu.edu.tr (O. Özenç) Geliş / Received: 29.07.2025 Kabul / Accepted: 02.10.2025 Yayımlanma / Published: 15.10.2025 doi: 10.28948/ngumuh.1753771

strategies is essential to achieving structural integrity and reliability under varied loading conditions. The importance of addressing these challenges cannot be overstated, as it is fundamental for preventing failures and improving the safety and performance of SHS-based structures [8,14,16–19]. Notably, the mass efficiency achieved through design optimization can increase the vulnerability of hollow sections to local buckling [3,20-22]. In addition to material properties and primary dimensions [23-25], the local and global buckling capacities of SHSs are substantially influenced by geometric imperfections and residual stresses arising from the manufacturing process [9,26,27]. In coldformed SHS columns, residual stresses differ based on manufacturing techniques, which are distinct from those applied in other structural components [28–30]. Two internationally recognized primary methods include direct forming, wherein a strip is roll-formed into an open section and welded along its edges, and continuous forming, in which a strip is initially roll-formed into a circular tube, welded, and subsequently flattened to achieve the desired rectangular shape [9]. Each technique exerts a substantial influence on the distribution and intensity of residual stresses in SHSs.

Box sections are often fabricated through the welding of four separate plates or by cold forming [31,32]. Welding is a technique used to fuse two or more materials together through localized melting followed by solidification [33]. Light and heavy welding are primarily differentiated by heat input and the resulting residual stress patterns [33,34]. Light welding involves lower heat input, typically achieved through reduced current and voltage, higher travel speed, short or intermittent welds, or single-pass techniques, resulting in smaller residual stresses, narrower heat-affected zones (HAZ), and minimal distortions. Heavy welding, in contrast, employs higher heat input through increased current and voltage, slower travel speed, continuous or multi-pass welds, producing larger weld beads, wider HAZs, and residual stresses that may approach the material's yield strength. These variations play a critical role in structural performance, as both the magnitude and distribution of welding-induced residual stresses strongly influence the local buckling resistance of thin-walled sections under axial compression. Light welding maintains lower stress levels and minimal distortion, whereas heavy welding induces pronounced tensile stresses near the weld and balancing compressive stresses elsewhere, significantly affecting structural stability. Early studies assumed that welded joints behaved elastically during welding; however, later theoretical and experimental research demonstrated that welding induces plastic deformation in surrounding areas, resulting in residual stresses upon cooling [35,36]. Subsequent investigations developed theoretical models for estimating welding-induced deformations in metals [37–40], revealing that residual stresses from welding can cause elastic buckling in plate elements and reduce the elastic buckling strength in center-welded plates with specific stress distributions [41]. Studies examining the impact of residual stresses on local buckling in welded box sections often employ models originally designed for plates. Residual

stresses are consistently shown in research to critically affect the buckling strength of centrally loaded steel columns, often triggering local buckling before global instability and leading to premature failure [42–45]. This detrimental effect is quantitatively confirmed by finite element simulations for axially compressed welded box sections, where residual stresses cause significant reductions in elastic buckling strength. The severity of this reduction is strongly correlated with the width-to-thickness ratio of the section walls [26].

Extensive analyses of residual stress distribution in welded SHSs reveal typical patterns: welding induces tensile stresses near corners and welds, with compressive stresses along plate mid-spans [46,47]. The magnitude and distribution of these stresses vary with welding parameters, including weld size, type, voltage, heat application, and the width-to-thickness ratio [9,48,49]. SHSs can manufactured using either low- or high-strength steel, with high-strength steel sections typically exhibiting greater buckling resistance, even though they possess higher levels of residual stress. Research suggests that buckling is influenced more by the residual-to-yield stress ratio than by absolute residual stress magnitude [9,50-52]. Additionally, studies confirm that compressive residual stress levels in high-strength steel sections are consistent across various steel grades [46,47,50,53].

Numerous studies have rigorously examined the effects of residual stresses on the buckling behavior of welded highstrength steel (HSS) box sections. For steels with strengths exceeding 600 MPa, findings suggest that tensile residual stresses along the weld bead may be lower than the yield strength of the base material [54]. Early research concentrated on HSS stub columns with yield strengths of 717 MPa and 800 MPa, plate thicknesses of 6.5 mm, and width-to-thickness ratios of 26.2 and 44, specifically addressing residual stress magnitudes and distributions [55] . Subsequent studies measured compressive residual stresses in welded box struts with 5 mm thick plates and yield strengths of 670 MPa and 705 MPa, covering width-tothickness ratios from 16 to 44 [56]. Additional research has assessed average residual stresses in various box sections fabricated from plates with thicknesses ranging from 4.5 mm to 6 mm and yield strengths between 568 MPa and 741 MPa. Studies have also examined residual stresses in HSS box sections with nominal yield strengths from 420 MPa to 1100 MPa [54].

While extensive research has characterized the influence of residual stresses on the local buckling strength of thicker-walled square hollow sections (SHSs) (wall thicknesses > 4.5 mm) under axial compression, the effects on thinner-walled SHSs subjected to alternative loading regimes remain inadequately investigated. This study addresses this knowledge gap through a parametric analysis of SHSs with a constant width-to-thickness ratio of 40, specifically focusing on pure major axis bending. By evaluating sections with thin walls (1 mm to 2.5 mm) and contrasting the consequences of high-magnitude versus low-magnitude welding-induced residual stress distributions, the research provides novel insights into their role in buckling behavior. Furthermore, by comparing the impact of residual stresses on

local elastic buckling under both major axis bending and axial compression, this work aims to refine structural design methodologies, potentially enabling more efficient and stable utilization of SHSs in critical engineering applications.

2 Theoretical background and calculations

2.1 Theory

The critical local elastic buckling stress (σ_{cr}) for members under any load can be determined using the well-known expression below [7,14,15,17,57].

$$\sigma_{cr} = k_{\sigma} \frac{\pi^2 E}{12(1 - v^2)} \left(\frac{t}{d}\right)^2 \tag{1}$$

where k_{σ} is the local elastic buckling coefficient and E is the elastic modulus. v represents the Poisson's ratio. d is the width of the relevant wall segment of a box section and t denotes the thickness of the relevant wall segment.

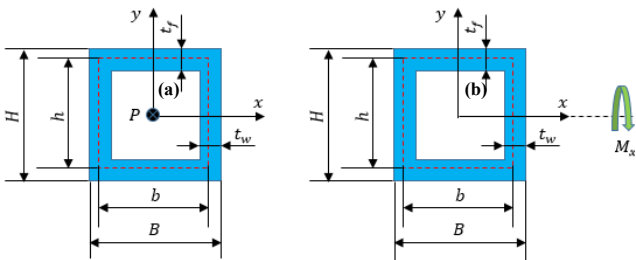


Figure 1. A Cross-Section of SHS Under Various Loads, (a) Axial Compression (P), (b) Major Axis Bending (M_r) .

Equation (1) can be rearranged for the SHSs illustrated in Figure 1, as follows [12,14,15,57]:

$$\sigma_{cr} = k_w \frac{\pi^2 E}{12(1 - v^2)} \left(\frac{t_w}{h}\right)^2$$

$$= k_f \frac{\pi^2 E}{12(1 - v^2)} \left(\frac{t_f}{b}\right)^2$$
(2)

where k_w and k_f are the local elastic buckling coefficient for the web and flange segments of the section, respectively. t_w and t_f represent the thickness of the web and flange segments of the section, respectively. b and b are the mid-line width and mid-line height of the section, respectively. These two parameters (b and b) can be defined as follows:

$$b = B - t_w \text{ and } h = H - t_f \tag{3}$$

where H is the height of the box section and B is the width of the box section, as illustrated in Figure 1. Note that in the case of square box sections with equal wall thickness $(t_w = t_f = t)$, the mid-line height h is equal to the mid-line width b, characteristic of SHS geometry (H = B).

Solving the equality given in Equation (2) yields the following expression, which relates the local elastic buckling

coefficient of the flange segment to that of the web segment [58].

$$k_f = k_w \left(\frac{b}{h}\right)^2 \left(\frac{t_w}{t_f}\right)^2 \tag{4}$$

Furthermore, in the case of $t_f = t_w = t$, Equation (4) reduces to

$$k_f = k_w \left(\frac{b}{h}\right)^2 \tag{5}$$

It is evident from Figure 1 that the mid-line width (b) equals the mid-line height (h), which is a fundamental geometric attribute of the square box section with equal wall thickness. Based on Equation 5, the relationship can be restated in the following manner.

$$k_f = k_w = k \tag{6}$$

Equation (2) is rearranged to highlight its simplification as follows:

$$\sigma_{cr} = k . n . \left(\frac{t}{H - t}\right)^2 \tag{7}$$

Here, *n* is the notation and represents $n = \frac{\pi^2 E}{12(1-v^2)}$.

The local elastic buckling coefficient k plays a pivotal role in determining the critical local elastic buckling stress σ_{cr} . The accuracy of σ_{cr} hinges directly on the precise value of k, underscoring the importance of comprehensively understanding this parameter. Despite the critical role it plays, there are limited studies available that focus specifically on determining k, which is influenced by factors such as boundary conditions, main dimensions of box section, and types of loading such as axial compression, major axis bending, minor axis bending, biaxial bending, and combined loading scenarios [15,57,58].

A noteworthy study presented an analytical expression for calculating the local elastic buckling coefficient of a flange segment of box section under axial compression (Figure 1(a)) with simply supported boundary conditions, as given below [57].

$$k_f = \frac{4}{\left(h/h\right)^{1.7}} \tag{8}$$

Equation (8) shows that k is always equal to 4 for SHSs subjected to axial compression since h = b. The same local buckling coefficient has also been reported for axially-compressed SHSs by several researchers [15,58]. It should be emphasized that the expression provided in Equation 8 is applicable solely to box sections with uniform wall thickness.

The local buckling coefficient of SHS subjected to major axis bending (Figure 1(a)) can be determined using an approximate formula derived by the notable study based on numerical analyses, as follows [15]:

$$k_w = P_{00} + \sum_{i=1}^4 P_{i0} (\varphi_w - 1)^i$$
 (9)

The unknown coefficients in Equation (9) are reported for SHS under pure major axis bending, as given below [15].

$$P_{00} = 4$$
, $P_{10} = -2.23$, $P_{20} = -1.585$, $P_{30} = -0.543$ and $P_{40} = -0.07$.

Additionally, φ_w ranging from -1 to 1 is associated with the magnitude of stresses at the flange-web mid-line corners arising from the applied moment. In the scenario of pure major axis bending, φ_w is equal to -1 ($\varphi_w = -1$) [15].

Substituting the above parameters into Equation (9) leads to k = 5.344.

Thus, the local elastic buckling coefficient of SHS under axial compression is determined to be $k_w = k_f = 4$, while for major axis bending, this value is found to be $k_w = k_f = k = 5.344$. Thus, for simplicity, the critical local elastic buckling stress definition given in Equation (7) can be rearranged for axial compression and major axis bending, respectively, as follows:

$$\sigma_{cr_Axial} = 4 . n . \left(\frac{t}{H - t}\right)^2 \tag{10}$$

$$\sigma_{cr_Bending} = 5.344 \cdot n \cdot \left(\frac{t}{H-t}\right)^2 \tag{11}$$

If the height-to-thickness ratio is maintained as constant $\frac{H}{t} = c$, both Equation (10) and Equation (11) can be expressed in the following forms.

$$\sigma_{cr_Axial} = 4 . n . \left(\frac{1}{c-1}\right)^2 \tag{12}$$

$$\sigma_{cr_Bending} = 5.344 \cdot n \cdot \left(\frac{1}{c-1}\right)^2 \tag{13}$$

Equation (12) highlights a fundamental insight: SHSs with identical c ratios have equivalent critical local elastic buckling stresses under axial compression. This observation underscores the essential role of geometric proportions in structural stability, independent of section dimensions. Moreover, regarding major axis bending, Equation (13) further elucidates how these geometric principles govern the buckling behavior of SHSs, providing a comprehensive framework for structural analysis and design.

Suppose the thickness and height of SHSs subjected to axial compression increase while maintaining a constant c. In that case, despite the critical local buckling stresses remaining the same, the critical local elastic buckling load increases due to the increase in the gross cross-sectional area and can be calculated using the following equation [57].

$$P_{cr} = \sigma_{cr \ Axial} . A_a \tag{14}$$

where A_g is the gross cross-sectional area of the SHS and can be calculated as given below.

$$A_g = 4t(H - t) \tag{15}$$

In the same manner, the critical local elastic buckling moment of the SHS subjected to major axis bending can be determined using the following expression [57].

$$M_{cr} = \sigma_{cr \ Bending} \cdot w_x \tag{16}$$

where w_x is the section modulus of the SHS about the x axis (Figure 1(b)) and can be determined as follows [57]:

$$w_x = \frac{H^3}{6} \left(1 - \left(\frac{H - 2t}{H} \right)^4 \right)$$
 (17)

2.2 Calculations for the critical local elastic buckling loads of SHSs.

The critical local elastic buckling stresses were calculated for SHSs with four varied cross-sectional dimensions, all maintaining a constant c=40, subjected to axial compression and major axis bending conditions. Table 1 presents the designation and geometric specifications of the SHSs discussed in the current study.

Table 1. The geometric specifications of SHSs addressed in the current study.

Specimen	H=B (mm)	t (mm)	L (mm)	c
SHS – 40 x 40 x 1	40	1	200	40
SHS – 60 x 60 x 1.5	60	1.5	300	40
$SHS-80 \ x \ 80 \ x \ 2$	80	2	400	40
SHS – 100 x 100 x 2.5	100	2.5	500	40

The SHSs are assumed to be fabricated from S235 steel grade, with the material properties for this grade provided in Table 2 [51].

Table 2. Material properties of S235 steel grade [51].

Material	E (MPa)	ν	σ _y (MPa)	σ _u (MPa)
S235	210000	0.3	282	324

Taking into account the cross-sectional dimensions of the samples listed in Table 1, the critical local elastic buckling stresses of SHSs under axial compressive load were computed using both Equation (10) and Equation (12). Following this, the corresponding bifurcation loads were calculated using Equation (14). The critical local elastic buckling stresses and bifurcation loads of SHSs under axial compression are shown in Table 3.

Table 3. The critical local elastic buckling stresses and corresponding bifurcation loads of SHSs under axial compression.

Specimen	с	n (MPa)	$\sigma_{cr_{Axial}} \\ (MPa)$	$\begin{matrix} A_g \\ (mm^2) \end{matrix}$	P _{cr} (kN)
SHS – 40 x 40 x 1	40	189800	498.64	156	77.788
SHS – 60 x 60 x 1.5	40	189800	498.64	351	175.022
$SHS-80\ x\ 80\ x\ 2$	40	189800	498.64	624	311.151
SHS – 100 x 100 x 2.5	40	189800	498.64	975	486.173

Similar to the axial compression loading case, the critical local elastic buckling stresses of SHSs subjected to bending were computed using both Equation (11) and Equation (13), with the corresponding bifurcation moments calculated using Equation (16). The results are presented in Table 4, detailing the critical local elastic buckling stresses and bifurcation moments of SHSs subjected to bending.

Table 4. The critical local elastic buckling stresses and corresponding bifurcation moments of SHSs under major axis bending.

	Specimen	c	n (MPa)	$\sigma_{\mathrm{cr}_{\mathrm{Bending}}}$ (MPa)	w _x (mm ³)	M _{cr} (kN.m)
	SHS – 40 x 40 x 1	40	189800	666.18	1978.6	1.318
	SHS – 60 x 60 x 1.5	40	189800	666.18	6677.8	4.448
	SHS – 80 x 80 x 2	40	189800	666.18	15828.8	10.544
2.5	SHS – 100 x 100 x	40	189800	666.18	30915.6	20.595

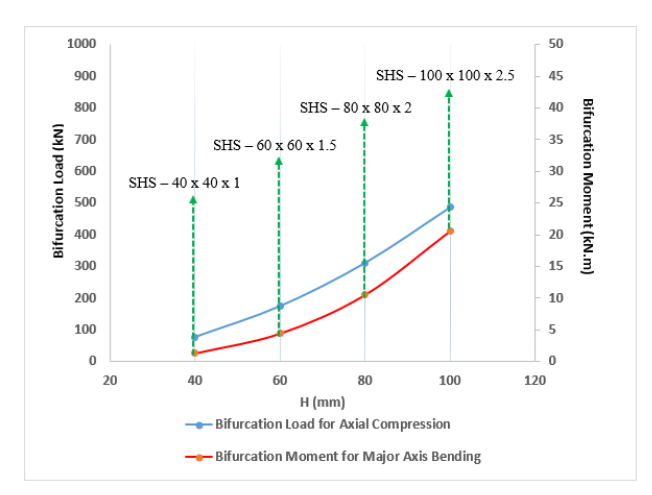


Figure 2. Bifurcation loads of SHSs with various cross-sectional dimensions under axial compression and major axis bending (c = 40 constant).

The critical local elastic buckling stresses of SHSs with identical c ratios under axial compression remain consistent across varying sizes, as detailed in Table 3. This consistency indicates that the geometric proportion (c) primarily governs the onset of buckling under axial compression. However, the bifurcation loads, also shown in Table 4, demonstrate an

increasing trend with the gross cross-sectional area of the SHSs. This suggests that while the critical buckling stress remains the same due to the same ratio of c, larger SHSs with greater cross-sectional areas can sustain higher bifurcation loads before structural failure. This principle also applies to major axis bending, where SHSs with the identical ratio c offer consistent critical local elastic buckling stresses across various sizes, as detailed in Table 4. However, the corresponding bifurcation moments increases with increasing section modulus as illustrated in Table 4. The graphical representations of the critical local elastic buckling loads for axial compression, as well as the critical local elastic moments for major axis bending, as presented in Table 3 and Table 4 respectively, are illustrated in Figure 2.

3 Finite element procedure

To validate the analytical calculations in this study, a linear elastic buckling analysis was conducted on SHSs subjected to axial compression and major axis bending, employing the Abaqus finite element software [59-61]. The accuracy of the finite element procedure was validated by comparing the analytically determined critical local elastic buckling loads of SHSs under both loading conditions with those extracted from the finite element analysis. These comparisons are discussed in detail in Section 3.6 (FEM Validation). Following the validation of the finite element procedure, the same methodology was employed to predict the influence of residual stress—resulting from light and heavy welding—on the local elastic buckling behavior of SHSs subjected to axial compression and major axis bending.

3.1 Finite element model configuration

The finite element model configuration for SHSs subjected to axial compression and major axis bending is illustrated in Figure 3. General-purpose 4-noded shell elements using reduced integration (S4R) were employed for grid discretization, as depicted in Figure 3. The S4R element type in Abaqus is highly versatile for simulating shell structures such as SHSs with varying thicknesses. With six degrees of freedom per node to capture translations and rotations, it accurately represents membrane, bending, and shear deformations [61–65]. The use of reduced integration balances computational efficiency and precision. This method, an early approach for estimating displacement and tension states within elements, incorporates higher-order polynomial functions to minimize finite element deformation errors [66,67]. Widely applied across engineering disciplines, it excels in analyzing structures under bending, buckling, and other loading conditions [68-70]. Attention to mesh refinement and aspect ratio control is crucial to ensure reliable results, particularly in areas with significant stress gradients or complex geometries. The S4R element type offers numerous advantages for buckling analysis of box sections. Its reduced integration scheme enhances computational efficiency while maintaining accuracy, making it suitable for comprehensive analyses. Moreover, the element effectively captures various buckling modes under diverse loading conditions, including compression, bending, and their combinations [12,68,71,72]. Due to its efficiency, the S4R element consistently provides precise predictions of critical buckling loads and modes, establishing it as a reliable choice across aerospace, automotive, and civil engineering sectors [12,61,70,73,74]. In summary, the S4R element type combines efficiency, precision, and adaptability, making it well-suited for buckling analysis applications involving SHSs in engineering.

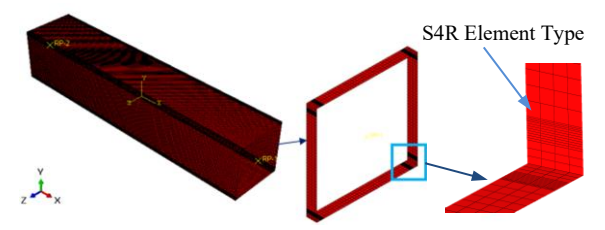


Figure 3. The mesh configuration of SHS discretized using the S4R element type.

3.2 Mesh configuration and density

In order to ensure the accuracy and reliability of the finite element procedure used in this study, a mesh convergence analysis was conducted on the SHS (SHS - 40 x 40 x 1) subjected to axial compression. Ensuring accuracy and reliability in finite element analysis necessitates meticulous attention to mesh refinement and aspect ratio control, especially in regions with significant stress gradients or complex geometries. The mesh was refined incrementally until the results stabilized, with further refinement showing minimal changes. This approach confirms that the finite element model can provide consistent and reliable predictions. This is particularly important for accurately capturing detailed stress distributions and buckling behavior under axial compression, ensuring the robustness and dependability of the analysis. The results obtained from the mesh convergence study are presented in Figure 4.

As demonstrated in Figure 4, the analysis results exhibit a clear convergence pattern as the mesh element size decreases below 6 mm. For the SHS regions not subjected to residual stress, a uniform mesh size of 1 mm was adopted. In contrast, for areas influenced by residual stresses, depicted

in Figure 2, the mesh was locally refined. Depending on whether heavy or light welding was simulated, element sizes in these regions were adjusted within the range of 0.2 mm to 0.5 mm, as illustrated in Figure 3.

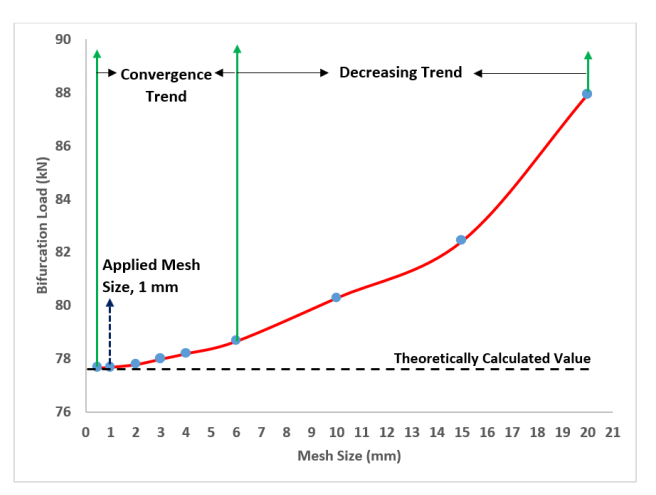


Figure 4. Results of the mesh convergence study.

3.3 Applied boundary constraints and load conditions

Two separate finite element models were constructed to simulate the loading scenarios of axial compression and major axis bending, as illustrated in Figure 5(a) and 5(b), respectively. A reference point was established at the center of each end of the SHS, serving as a control node. For the axial compression case, these points were linked to the SHS ends via kinematic couplings, while for major axis bending, rigid body-pin connections were employed, consistent with the methods outlined in [17,61]. Each loading condition was analyzed independently, with corresponding boundary constraints applied to the designated reference points. A unit axial load was imposed and transferred to the SHS for the compression model, whereas a unit moment was applied in the bending case. The boundary and loading configurations for each scenario are presented in Figures 5(a) and 5(b), respectively. This modeling setup allows for accurate representation of the loading mechanisms and supports the validation of the finite element approach

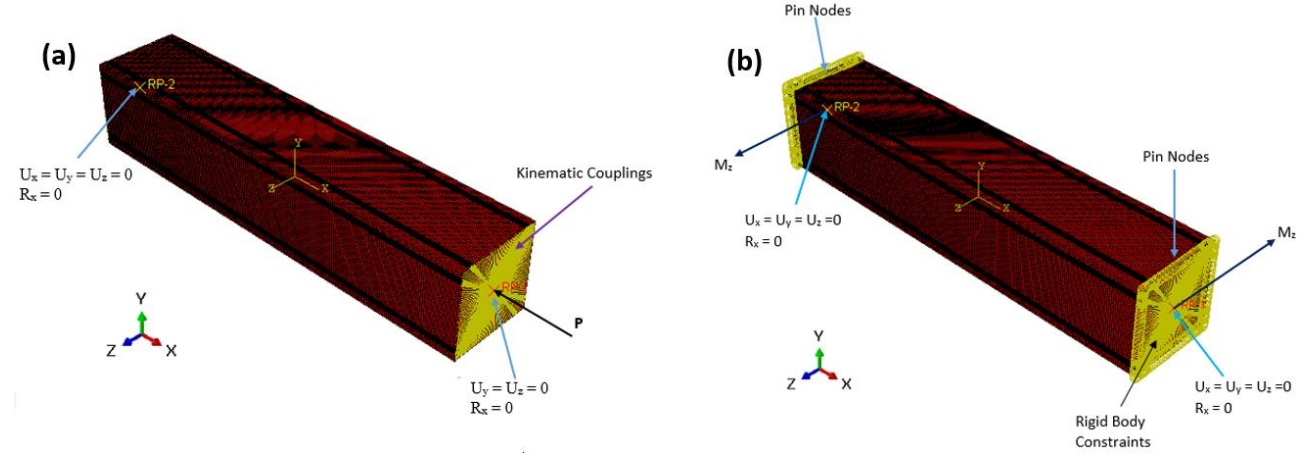


Figure 5. Boundary and loading conditions employed in the simulations, (a) Axial compression, (b) Major axis bending.

3.4 Analysis methodology and material properties

Linear elastic eigenvalue buckling analysis, commonly referred to as bifurcation analysis, is used to assess the theoretical buckling strength of structures by identifying bifurcation points and associated failure modes through a linearized model [75]. Thus, the critical local elastic buckling loads and moments, indicative of the first local buckling mode, were extracted for each SHS through this analysis. The Lanczos eigen-solver, a robust method for computing extreme eigenvalues and their associated eigenvectors, was utilized to obtain these parameters [73,76]. The SHSs were assumed to be fabricated from S235 steel, with material properties outlined in Table 2, including an elastic modulus of 210 GPa and Poisson's ratio of 0.3 [51].

3.5 Applying residual stress

The residual stress distribution for an SHS welded at all four corners, as specified by the relevant design code [48], is illustrated in Figure 6.

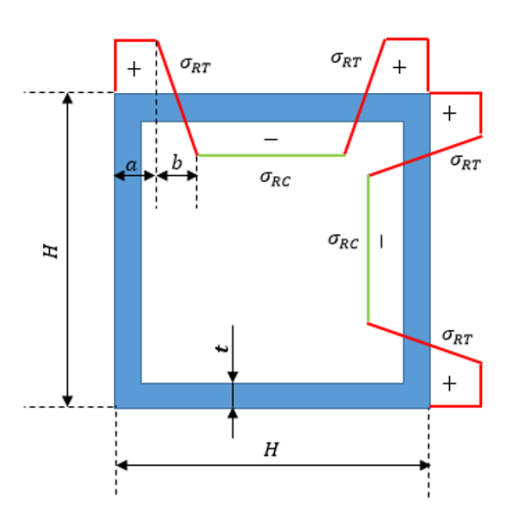


Figure 6. The residual stress distribution for an SHS welded at all four corners [48].

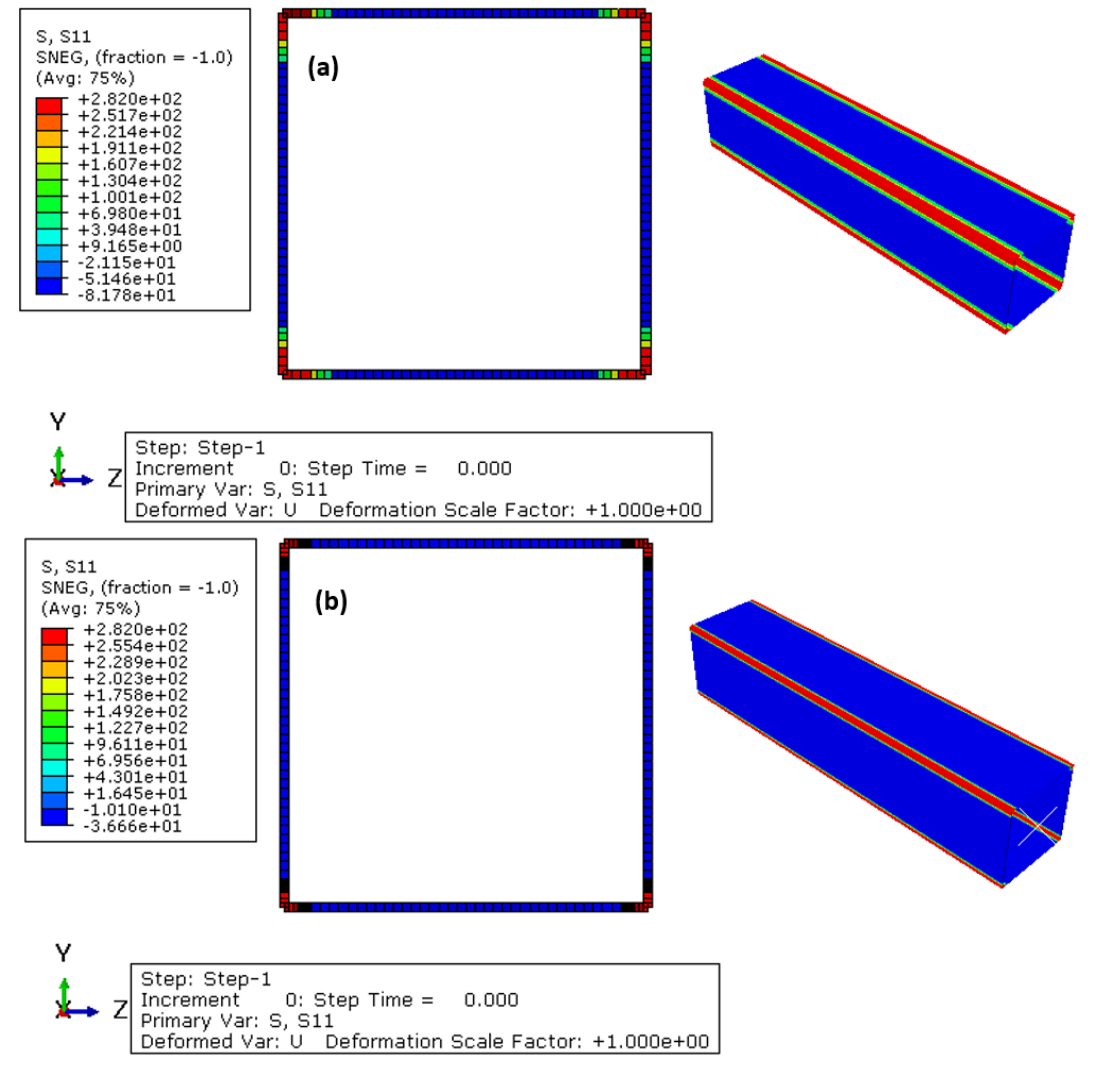


Figure 7. The residual stress distribution in SHS for various welding types, (a) Heavy welding, (b) Light welding

In Figure 6, σ_{RT} and σ_{RC} represent the residual tensile stress and residual compressive stress, respectively. The magnitudes of these stresses vary according to the welding type and the ratio of c. These variations underscore the influence of welding techniques and geometric proportions on the distribution of residual stresses in SHSs. Given that this study is limited to SHSs with heavy and light welding at all four corners and a constant ratio of c=40, the relevant relations for determining these parameters are presented in Table 5.

Table 5. Parameters for the determination of the residual stress distribution in SHS [48,51].

c	Welding Type	σ_{RT}/σ_y	σ_{RC}/σ_y	а	b
40	Heavy Weld	1	-0.29	3t	3t
40	Light Weld	1	-0.13	1.5 <i>t</i>	1.5t

Note that the parameter σ_y in Table 5 signifies the yield strength of the material employed in producing the SHS.

Considering the values given in Table 5, the residual stresses have been effectively applied to the SHSs for both heavy welding and light welding conditions. The resulting distribution of residual stress for heavy and light welding is depicted in Figure 7(a) and 7(b), respectively.

3.6 FEM validation

The finite element procedure adopted in this study has been rigorously validated by comparing the theoretically calculated critical local elastic buckling loads of SHSs under axial compression and major axis bending with numerical predictions. This validation affirmed the robustness and precision of the finite element model in predicting buckling behavior. Following validation, the same rigorous procedure was applied to SHSs incorporating residual stress effects, thereby bolstering the credibility of the analytical techniques utilized in this investigation.

The predicted critical local elastic buckling modes and their corresponding bifurcation loads for axially compressed SHSs with varying cross-sectional dimensions but the identical ratio of c=40 are depicted in Figure 8. Notably, the predicted local elastic buckling mode shapes have been found to be consistent with those reported for SHSs under axial compression [7,15]. This confirms the accuracy and dependability of the simulation model in accurately representing local elastic buckling mode shapes of SHSs subjected to axial compression.

The comparison between theoretical and numerical bifurcation loads for SHS specimens under axial compression, as presented in Table 6, demonstrates a high level of agreement with percentage errors ranging from 0.01513% to 0.01577%, affirming the accuracy and reliability of the finite element analysis method employed.

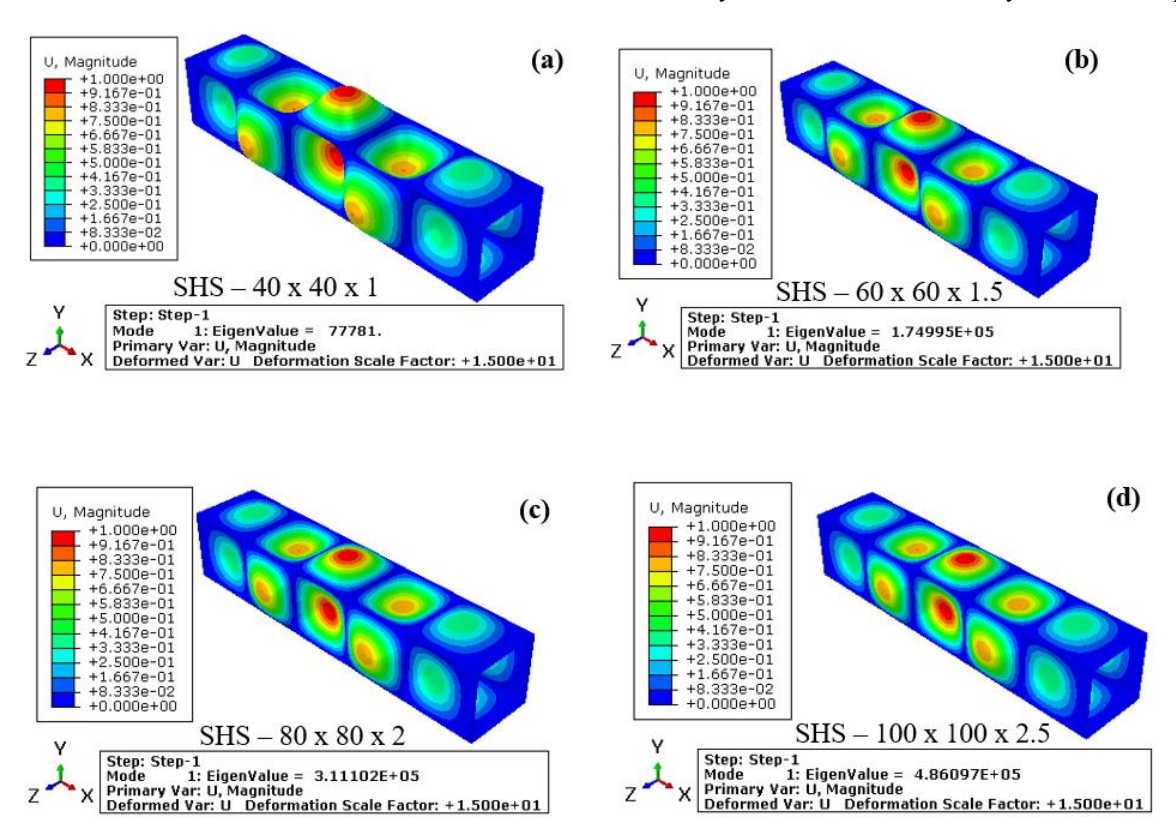


Figure 8. The critical local elastic buckling modes and corresponding bifurcation loads af axially compressed SHSs with various cross-section dimensions, (a) SHS $-40 \times 40 \times 1$, (b) SHS $-60 \times 60 \times 1.5$, (c) SHS $-80 \times 80 \times 2$, and (d) SHS $-100 \times 100 \times 2.5$.

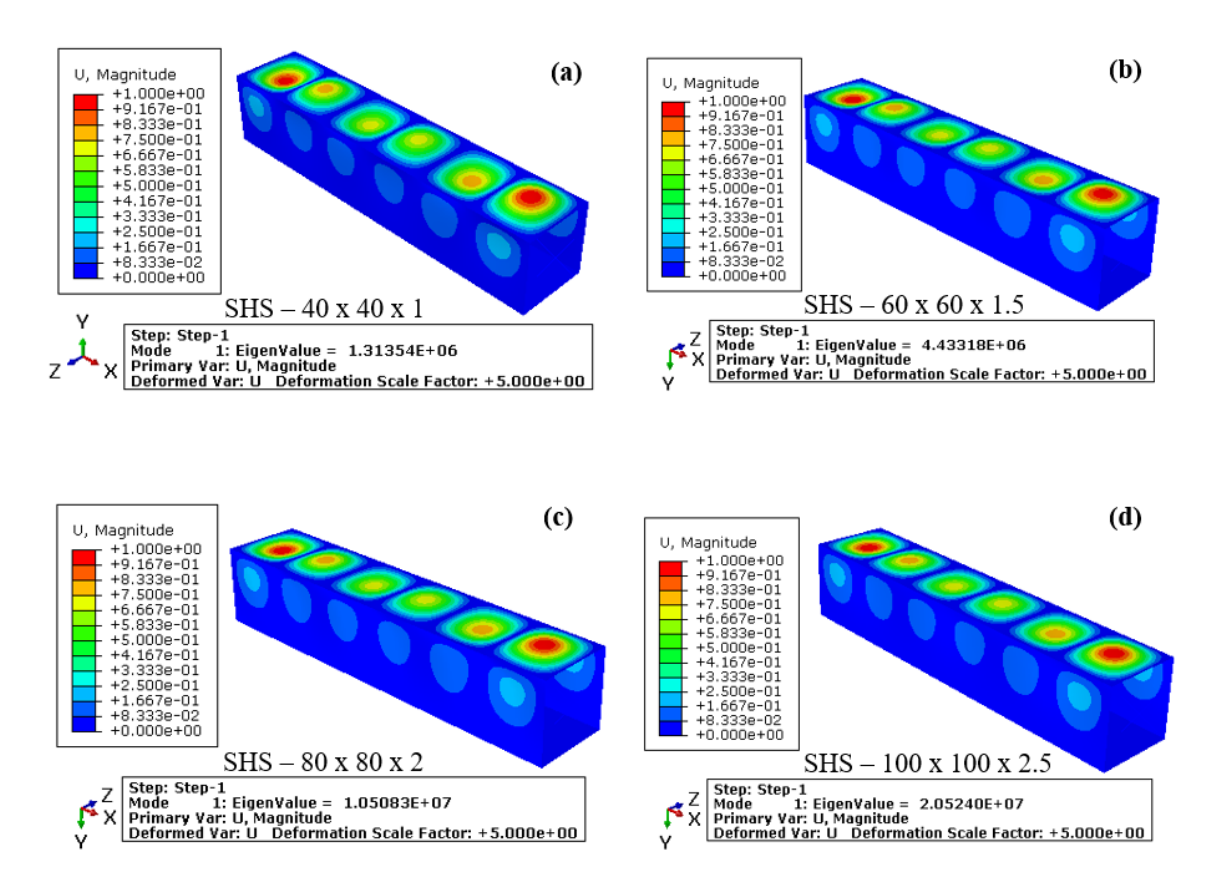


Figure 9. The critical local elastic buckling modes and corresponding bifurcation moments af SHSs with various cross-section dimensions under major axis bending: (a) SHS – 40 x 40 x 1, (b) SHS – 60 x 60 x 1.5, (c) SHS – 80 x 80 x 2, and (d) SHS – 100 x 100 x 2.5.

Table 6. Theoretical and numerical comparison of bifurcation loads for SHSs under axial compression.

Cucaimon	Bifurcation	Error %	
Specimen	Theoretical	Numerical	Error 70
SHS – 40 x 40 x 1	77.787	77.776	0.0141
$SHS - 60 \times 60 \times 1.5$	175.022	174.995	0.0154
$SHS - 80 \times 80 \times 2$	311.151	311.102	0.0157
SHS – 100 x 100 x 2.5	486.173	486.097	0.0156

Table 7. Theoretical and numerical comparison of bifurcation moments for SHSs under major axis bending.

Cucaimon	Bifurcation M	Error	
Specimen	Theoretical	Numerical	%
SHS – 40 x 40 x 1	1.318	1.313	0.379
$SHS - 60 \times 60 \times 1.5$	4.448	4.433	0.337
$SHS - 80 \times 80 \times 2$	10.544	10.508	0.341
SHS – 100 x 100 x 2.5	20.595	20.524	0.344

Figure 9 presents the anticipated critical local elastic buckling modes and their associated bifurcation moments for SHSs addressed. The predicted mode shapes closely mirror those documented in previous investigations of SHSs under similar bending conditions [12,15,17], underscoring the fidelity of the simulation model in characterizing local elastic buckling phenomena of SHS under major axis bending.

The comparison in Table 7 between theoretical and numerical bifurcation moments for SHSs under major axis bending shows a very low percentage error (around 0.35%),

indicating strong agreement between theoretical calculations and numerical simulations.

The comparison between theoretical and numerical bifurcation loads for SHS specimens under axial compression, as presented in Table 6, demonstrates a high level of agreement with percentage errors ranging from 0.01513% to 0.01577%, affirming the accuracy and reliability of the finite element analysis method employed. In essence, not only was the finite element procedure in this study validated against theoretical results of SHS under axial compression, but it was also verified for SHS under major axis bending, encompassing element type, mesh density, boundary conditions, and loading conditions. Consequently, the same finite element procedure has been applied to parametrically investigate the effects of residual stress on the local elastic buckling behavior of SHSs under axial compression and major axis bending.

4 Results of the parametric study and discussions

This section details the outcomes of a parametric study investigating the effects of residual stress, induced by heavy and light welding at the four corners of SHS, on the local elastic buckling behavior of SHS under axial compression and major axis bending. By investigating varying welding intensities, this study seeks to offer a nuanced understanding of their effects on the structural stability and buckling performance of SHSs under different loading conditions.

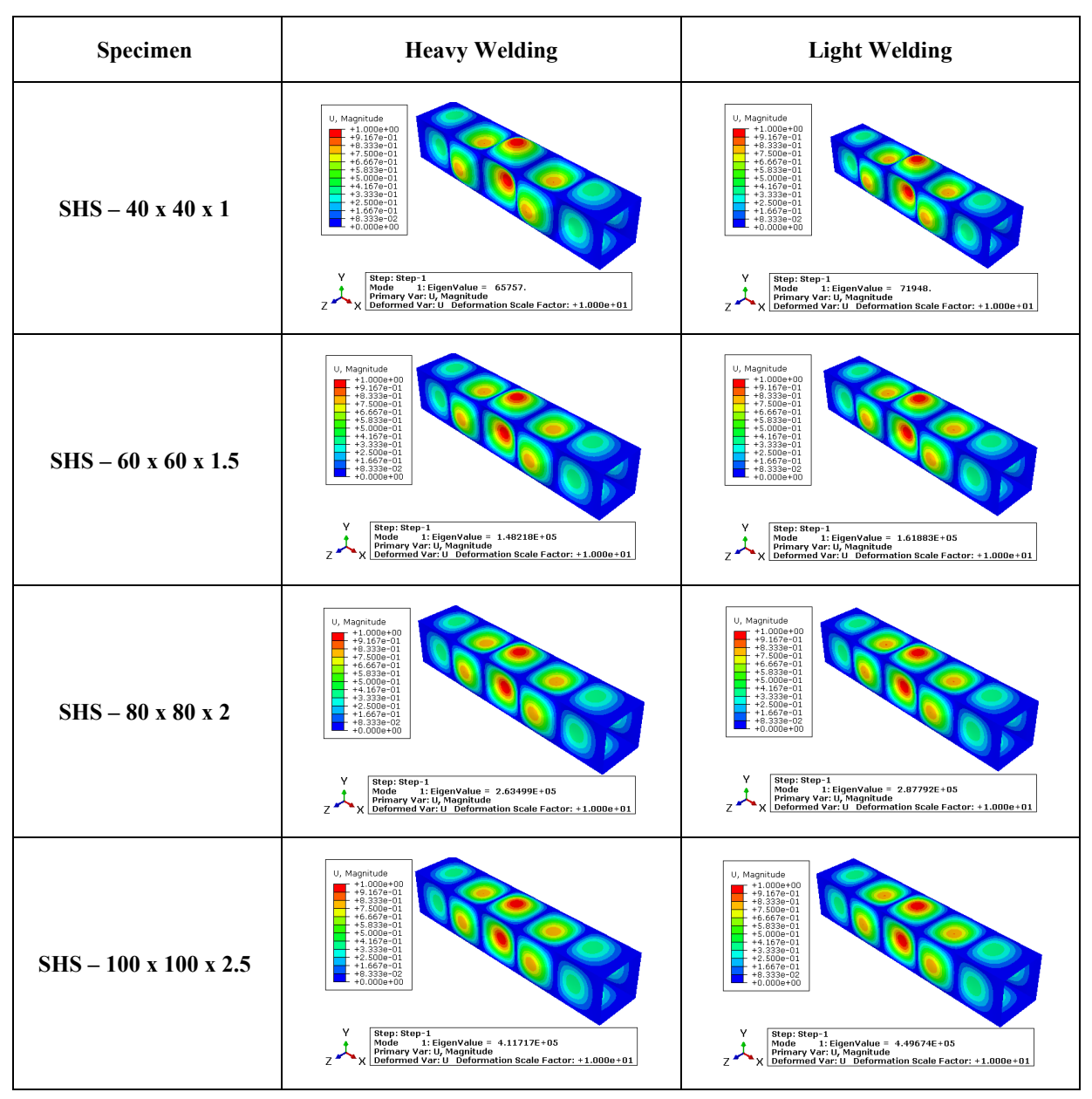


Figure 10. The predicted linear elastic buckling modes and corresponding bifurcation loads of SHSs subjected to axial compression, welded at four corners with varying welding types.

4.1 Axial compression

The predicted linear elastic buckling modes and corresponding bifurcation loads of SHSs subjected to axial compression, welded at four corners with heavy and light welding, are illustrated in Figure 10. As illustrated in Figure 10, while the residual stress distribution and its magnitude vary with welding type, these variations do not influence the linear elastic local buckling modes of SHSs. However, the critical local elastic buckling loads are notably compromised by the presence of residual stress, particularly more pronounced in heavy welding compared to light welding.

The results presented in Table 8 show that the bifurcation loads of SHS specimens under axial compression decrease notably with the presence of residual stress induced by welding at the corners. For instance, in the smallest SHS (40

x 40 x 1), the bifurcation load decreases by approximately 7.5% with light welding and by about 15.3% with heavy welding compared to the scenario without residual stress. This trend continues across larger specimens, with similar percentage decreases observed. The findings highlight that residual stress, particularly from heavy welding, significantly compromises the structural integrity of SHSs, reducing their critical load-bearing capacity. This underscores the importance of carefully managing welding practices to mitigate adverse effects on the buckling behavior and overall performance of SHS structures under axial compression.

		Bifurcation Load (kN)			Decrease (%)	
Specimen	Without Residual Stress	With Residual Stress (Light Welding)	With Residual Stress (Heavy Welding)	Light Welding	Heavy Welding	
SHS – 40 x 40 x 1	77.776	71.948	65.876	7.49%	15.3%	
SHS – 60 x 60 x 1.5	174.995	161.883	148.218	7.49%	15.3%	
SHS – 80 x 80 x 2	311.102	287.792	263.499	7.49%	15.3%	
SHS – 100 x 100 x 2.5	486.097	449.674	411.717	7.49%	15.3%	

Table 8. Effect of residual stress from different welding types on bifurcation loads of SHSs under axial compression.

The results in Figure 11 clearly highlights the influence of residual stress from two different welding types on the critical local elastic buckling loads of SHSs under axial compression across varying thicknesses but the identical c=40. Regardless of thickness, the presence of residual stress reduces the bifurcation load, with heavy welding causing a more pronounced reduction compared to light welding. This is mainly due to the reduction in local buckling load capacity being more significantly influenced by the ratio of residual stress to yield stress than by the absolute magnitude of residual stresses (Table 5).

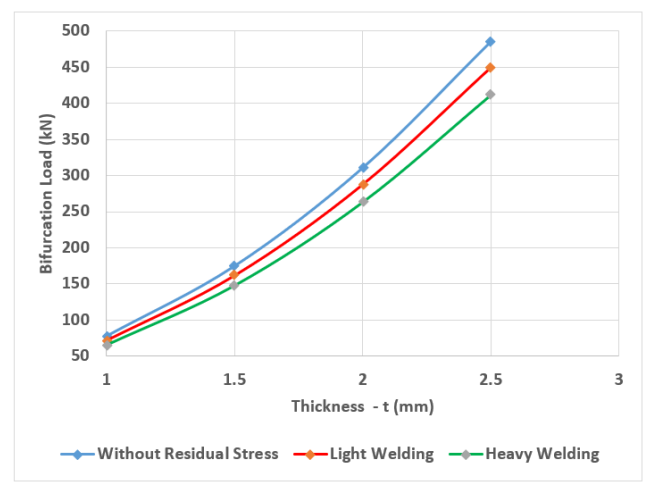


Figure 11. The influence of residual stress from different welding types on the critical local elastic buckling load of SHSs under axial compression, (c=40 constant).

It is important to note that, while the critical local elastic buckling loads enhance with increasing thickness, the critical local elastic buckling stresses remain unchanged because the gross cross-sectional area increases proportionally with thickness. The critical local elastic buckling stresses of SHSs under axial compression have been parametrically investigated for light welding (461.20 MPa) and heavy welding (422.28 MPa), compared to the baseline without residual stress (498.56 MPa). Notably, these stress values remain consistent regardless of the thickness of the SHSs. This study underscores that both light and heavy welding processes uniformly introduce residual stresses that reduce the buckling resistance of SHSs. The higher initial buckling

resistance observed without residual stress highlights the significant influence of welding-induced residual stresses on the structural stability of SHSs. Managing these residual stresses is crucial for optimizing the performance and reliability of SHSs under compressive loads in engineering applications.

For simplicity, the following expressions have been developed from the data in Table 8 to quantify the critical local elastic buckling loads of axially compressed SHSs, taking into account different welding conditions and the absence of residual stress.

For the absence of residual stress:

$$P_{cr_Axial_No_Residual} = 16.n. \left(\frac{t^2}{39}\right)$$
 (18)

For the residual stress arising from light welding:

$$P_{cr_Axial_Light_Weld} = 0.9256 * P_{cr_Axial_No_Residual}$$
 (19)

For the residual stress arising from heavy welding:

$$P_{cr_Axial_Heavy_Weld} = 0.8467 * P_{cr_Axial_No_Residual}$$
 (20) where $n = \frac{\pi^2 E}{12(1-v^2)}$.

Emphasizing their specificity, the above equations are designed to assess the critical local elastic buckling of axially compressed SHSs with all four corners welded, while maintaining a constant c=40.

4.2 Major axis bending

Figure 12 depicts the linear elastic buckling modes and corresponding bifurcation moments for SHSs under major axis bending, with all four corners welded using either heavy or light welding. The data indicate that while the distribution and magnitude of residual stress differ depending on the welding type, these differences do not alter the fundamental linear elastic buckling modes of the SHSs. However, the critical local elastic buckling moments are notably reduced due to residual stress, with the reduction being more severe in the case of heavy welding compared to light welding. This suggests that while the overall shape of the buckling modes remains consistent, the ability of the SHSs to withstand bending moments is compromised by the residual stresses introduced during welding.

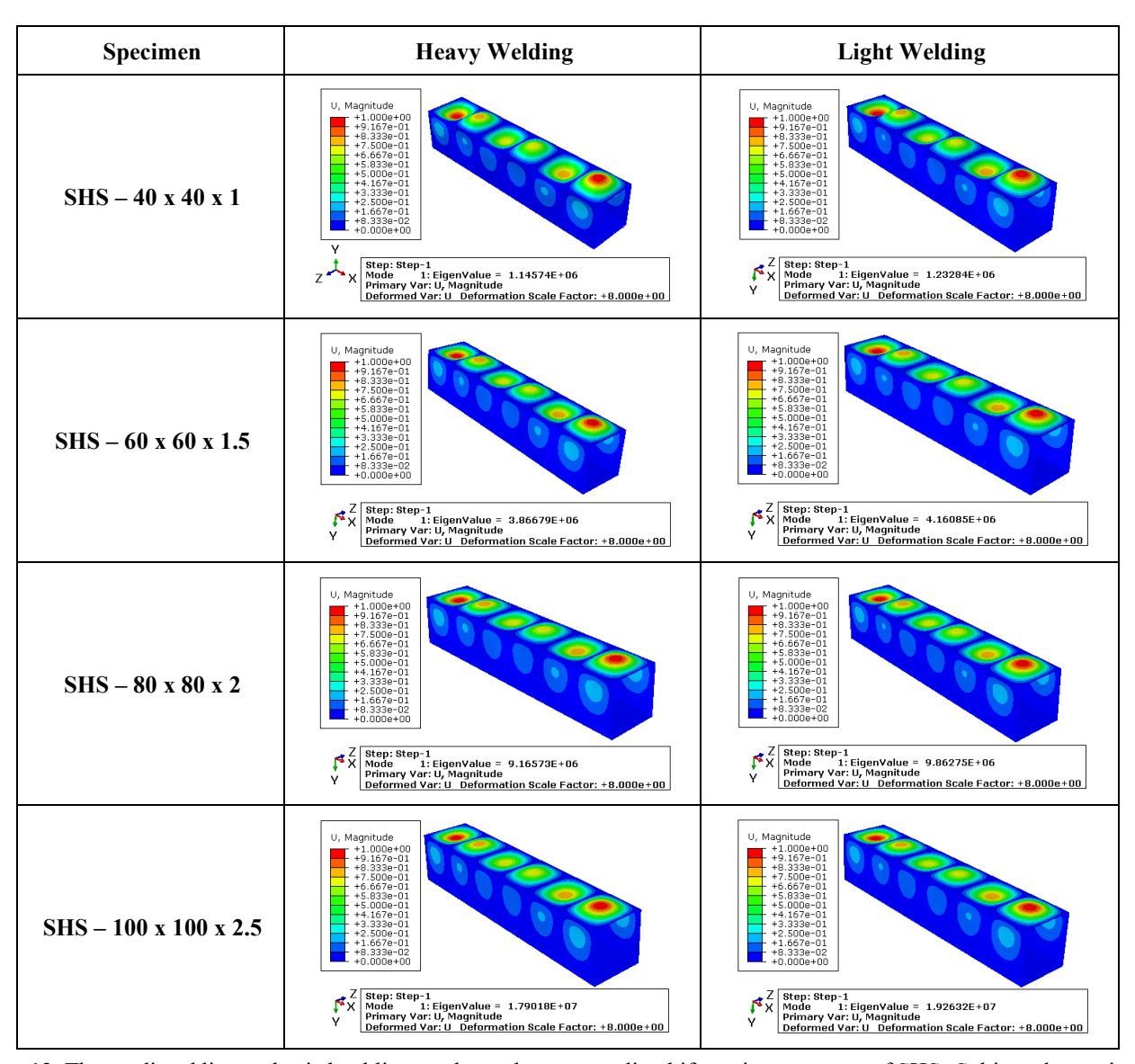


Figure 12. The predicted linear elastic buckling modes and corresponding bifurcation moments of SHSs Subjected to major axis bending, welded at four corners with varying welding types.

The results reported in Table 9 illustrates a notable decrease in the bifurcation moments of SHS specimens under major axis bending due to residual stress induced by welding at all four corners. For instance, in SHS specimens with a constant c = 40, such as those described, the bifurcation moment decreases by approximately 6.14% with light welding and 12.78% with heavy welding compared to scenarios without residual stress. This percentage decrease remains constant across SHSs of larger dimensions within the constant ratio of c = 40. These findings underscore how stress, particularly from heavy welding, significantly compromises the structural integrity of SHSs, reducing their critical moment-bearing capacity irrespective of their specific cross-sectional size within the c = 40. Therefore, careful management of welding practices is essential to mitigate these adverse effects on the buckling behavior and overall performance of SHS structures under major axis bending.

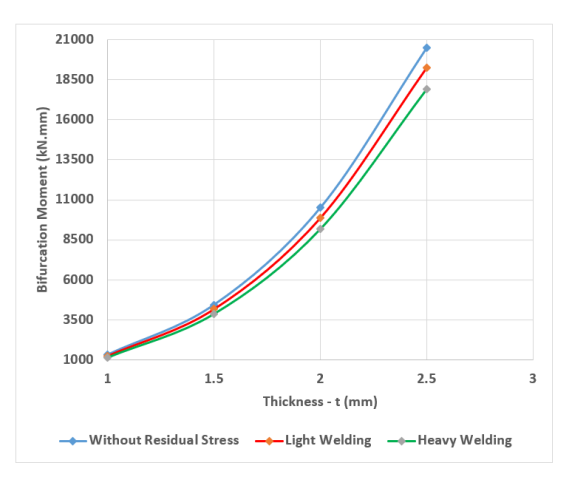


Figure 13. The influence of residual stress from different welding types on the critical local elastic buckling moments of SHSs under major axis bending, (H/t=40 constant).

	1	Bifurcation Moment (kN.m)			
Specimen	Without Residual Stress	With Residual Stress (Light Welding)	With Residual Stress (Heavy Welding)	Light Welding	Heavy Welding
SHS – 40 x 40 x 1	1.313	1.232	1.145	6.17%	12.79%
SHS – 60 x 60 x 1.5	4.433	4.160	3.866	6.16%	12.79%
SHS – 80 x 80 x 2	10.508	9.862	9.165	6.15%	12.78%
SHS – 100 x 100 x 2.5	20.524	19.263	17.901	6.14%	12.78%

Table 9. Effect of residual stress from different welding types on bifurcation moments of SHSs under major axis bending.

The results in Figure 13 clearly illustrate how residual stress from two different welding types influences the critical local elastic buckling moments of SHSs under major axis bending, maintaining a constant c=40 across varying thicknesses. Despite differences in thickness, the presence of residual stress consistently reduces the bifurcation moments, with heavy welding causing a more pronounced reduction compared to light welding. This reduction is primarily influenced by the ratio of residual stress to yield stress (Table 5), highlighting its critical role in diminishing the local buckling moment capacity of SHSs.

The critical local elastic buckling stresses, as calculated from Table 9, are 664 MPa without residual stress, 623 MPa with light welding, and 579 MPa with heavy welding. These values remain consistent as the critical local elastic buckling moments increase with thickness, due to the proportional increase in section modulus. Residual stresses from both light and heavy welding consistently diminish the buckling resistance of SHSs, underscoring the importance of managing these stresses for reliable performance and durability in major axis bending applications.

To simplify, the following expressions have been derived from the data in Table 8 to quantify the critical local elastic buckling moments of SHSs under major axis bending, considering various welding conditions and without residual stress

For the absence of residual stress:

$$M_{cr_Bending_No_Residual} = 6.95. n. t^{3}$$
 (21)

For the residual stress arising from light welding:

$$M_{cr_Bending_Light_Welding}$$

= 0.9369
* $M_{cr_Bending_No_Residual}$ (22)

For the residual stress arising from heavy welding:

$$M_{cr_bending_Heavy_Welding}$$

= 0.8695
* $M_{cr_Bending_No_Residual}$ (23)

where
$$n = \frac{\pi^2 E}{12(1-v^2)}$$
.

Highlighting their applicability, the equations above are tailored for evaluating the critical local elastic buckling of SHSs under major axis bending, with all four corners welded and a constant c = 40.

In essence, in axial compression (bifurcation load), light welding leads to a reduction of approximately 7.5%, whereas heavy welding results in a more substantial decrease of around 15.3%. Comparatively, under major axis bending (bifurcation moment), light welding causes a reduction of about 6.14%, while heavy welding results in a decrease of approximately 12.78%. This highlights how residual stresses significantly diminish the load-carrying capacity of SHSs, with axial compression showing a more pronounced effect. Accurately accounting for the residual stress effects on the load-carrying capacities of these SHSs in numerical simulations is crucial for precise predictions and robust design.

5 Concluding remarks

The findings of the parametric studies led to the following conclusions.

- Residual stresses induced by welding, especially heavy welding, significantly reduce the critical load-bearing capacities of SHSs under both axial compression and major axis bending. This is primarily due to high-magnitude compressive residual stresses induced by heavy welding as shown in Table 5. The substantial heat input causes widespread thermal plastic deformation; subsequent constrained shrinkage generates compressive stresses in stability-critical zones like the mid-regions of flanges and webs as presented in Figure 6. These residual stresses act as a pre-load, superimposing with service stresses to promote premature yielding, which reduces effective stiffness and elastic buckling resistance. Consequently, both axial buckling capacity and bending moment resistance are diminished, with the severity scaling directly with heat input, making heavily welded SHSs notably more vulnerable than lightly welded or non-welded members.
- In axial compression, the bifurcation loads decrease by approximately 7.5% with light welding and 15.3% with heavy welding across different SHS sizes. Comparatively, under major axis bending, the bifurcation moments decrease by about 6.14% with light welding and 12.78% with heavy welding. This indicates a slightly more pronounced

reduction in load-carrying capacity due to residual stress in axial compression scenarios.

- The percentage decrease in load-bearing capacity remains relatively consistent across different SHS sizes within the study's parameters, emphasizing the universal impact of residual stresses on structural stability.
- Not only does residual stress not affect the local elastic buckling modes of SHSs under axial compression, but it also has no influence under major axis bending.
- Heavy welding induces higher residual stresses (residual stress to yield strength ratio) compared to light welding. These residual stresses act as imperfections in the material, reducing its load-carrying capacity by initiating buckling at lower loads or moments.
- The ratio of residual stress to yield strength plays a more important role in reducing the load-carrying capacity of SHSs than the actual distribution of residual stresses. This ratio determines how much the residual stresses can weaken the material, leading to a substantial reduction in both critical buckling loads and moments.
- The equations derived for calculating bifurcation loads and moments (such as Equations (18), (19), (20) for axial compression, and (21), (22), (23) for major axis bending) show that both types of welding introduce reduction factors (0.9256 for light welding and 0.8467 for heavy welding in axial compression, and 0.9369 for light welding and 0.8695 for heavy welding in bending). These reduction factors directly reflect how residual stresses decrease the effective capacity of the SHS to resist buckling. These equations quantify the critical local elastic buckling loads and moments of SHSs, incorporating the effects of residual stresses due to different welding conditions. The significant reduction factors for heavy welding reflect the crucial role of the residual stress to yield strength ratio in diminishing the load-carrying capacity of SHSs. This ratio, rather than the mere distribution of residual stresses, is pivotal in determining the extent of structural performance reduction.
- The derived equations are specifically applicable for determining the critical local elastic buckling loads of SHSs with all four corners welded, under axial compression and major axis bending, and having a constant c = 40.
- The derived equations provide a quantitative framework to understand and predict these effects, essential for optimizing welding practices and ensuring the structural reliability of SHSs in engineering applications.
- This parametric study helps designers optimize the design and safety of SHS structures by offering critical insights into the impact of residual stresses arising from different welding intensities, such as heavy and light welding. By emphasizing the crucial role of the residual stress to yield strength ratio, the study enhances predictive accuracy, guides effective welding practices, and ensures compliance with regulatory standards. Additionally, it improves material efficiency and structural integrity while laying the groundwork for future research, significantly contributing to advancements in the field of structural engineering.

Conflicts of interest

The authors declare that there are no conflicts of interest.

Similarity rate (iThenticate): 19 %

References

- [1] P.W. Key and G.J. Hancock, A theoretical investigation of the column behaviour of cold-formed square hollow sections, Thin-Walled Structures. 16, 31–64, 1993. https://doi.org/10.1016/0263-8231(93)90040-H.
- [2] J. Shen and M.A. Wadee, Local-global mode interaction in thin-walled inelastic rectangular hollow section struts part 2: Assessment of existing design guidance and new recommendations, Thin-Walled Structures. 145, 106184, 2019. https://doi.org/10.1016/j.tws.2019.106184.
- [3] J. Shen and M.A. Wadee, Local–global mode interaction in thin-walled inelastic rectangular hollow section struts part 1: Nonlinear finite element analysis, Thin-Walled Structures. 145, 106183, 2019. https://doi.org/10.1016/j.tws.2019.106183.
- [4] R.G. Zhao, R.F. Huang, H.A. Khoo, and J.J.R. Cheng, Experimental study on slotted rectangular and square hollow structural section (HSS) tension connections, Canadian Journal of Civil Engineering. 35, 1318–1330, 2007. https://doi.org/10.1139/L08-069.
- [5] T.G. Singh and T.-M. Chan, Effect of access openings on the buckling performance of square hollow section module stub columns, Journal of Constructional Steel Research. 177, 106438, 2021. https://doi.org/10.1016/j.jcsr.2020.106438.
- [6] J. Wardenier, J.A. Packer, X.-L. Zhao, and G.J. Van der Vegte, Hollow sections in structural applications, Bouwen met staal Rotterdam, The Netherlands, 2002.
- [7] M.A. Dundar and M. Nuraliyev, Parametric study on the assessment of the local buckling behavior of perforated square hollow sections with non-uniform wall thickness under axial compression TT Düzgün olmayan duvar kalınlığına sahip delikli kare içi boş profillerin eksenel basınç alt, Journal of Innovative Engineering and Natural Science. 4, 326–353, 2024. https://doi.org/10.61112/jiens.1397391.
- [8] B. Kövesdi and B. Somodi, Buckling resistance of HSS box section columns part I: Stochastic numerical study, Journal of Constructional Steel Research. 140, 1–10, 2018. https://doi.org/10.1016/j.jcsr.2017.10.016.
- [9] I. Quillupangui, B. Somodi, and B. Kövesdi, Overview of FEM-Based Resistance Models for Local Buckling of Welded Steel Box Section Columns, Applied Sciences. 14, 2024. https://doi.org/10.3390/app14052029.
- [10] J. Wardenier, D. Dutta, and N. Yeomans, Design guide for structural hollow sections in mechanical applications, Verlag TÜV Rheinland, 1995.
- [11] J. Wardenier, Hollow Sections in Structural Applications. CIDECT, Netherlands, 2000.
- [12] M. Nuraliyev, M.A. Dundar, and D.E. Sahin, Determination of optimal dimensions of polymer-based rectangular hollow sections based on both adequatestrength and local buckling criteria: Analytical and

- numerical studies, Mechanics Based Design of Structures and Machines. 1–31, 2022. https://doi.org/10.1080/15397734.2022.2139720.
- [13] H.X. Yuan, Y.Q. Wang, L. Gardner, and Y.J. Shi, Local—overall interactive buckling of welded stainless steel box section compression members, Engineering Structures. 67, 62–76, 2014. https://doi.org/10.1016/j.engstruct.2014.02.012.
- [14] L. Gardner, A. Fieber, and L. Macorini, Formulae for Calculating Elastic Local Buckling Stresses of Full Structural Cross-sections, Structures. 17, 2–20, 2019. https://doi.org/10.1016/j.istruc.2019.01.012.
- [15] L. Vieira, R. Gonçalves, and D. Camotim, On the local buckling of RHS members under axial force and biaxial bending, Thin-Walled Structures. 129, 10–19, 2018. https://doi.org/10.1016/j.tws.2018.03.022.
- [16] A. Saoula, S.A. Meftah, F. Mohri, and E.M. Daya, Lateral buckling of box beam elements under combined axial and bending loads, Journal of Constructional Steel Research. 116, 141–155, 2016. https://doi.org/10.1016/j.jcsr.2015.09.009.
- [17] M. Nuraliyev, M.A. Dundar, and H.K. Akyildiz, A novel analytical method for local buckling check of box sections with unequal wall thicknesses subjected to bending, Mechanics of Advanced Materials and Structures. 1–24, n.d. https://doi.org/10.1080/15376494.2024.2369262.
- [18] O. Zhao, B. Rossi, L. Gardner, and B. Young, Behaviour of structural stainless steel cross-sections under combined loading Part II: Numerical modelling and design approach, Engineering Structures. 89, 247–259, 2015. https://doi.org/10.1016/j.engstruct.2014.11.016.
- [19] C.D. Moen and B.W. Schafer, Elastic buckling of cold-formed steel columns and beams with holes, Engineering Structures. 31, 2812–2824, 2009. https://doi.org/10.1016/j.engstruct.2009.07.007.
- [20] F.I. NIORDSON, ed., CHAPTER 17 Buckling of Plates and Shells, in: North-Holland Series in Applied Mathematics and Mechanics, North-Holland, 1985: pp. 383–398. https://doi.org/10.1016/B978-0-444-87640-9.50023-X.
- [21] L. Gardner and D.A. Nethercot, Experiments on stainless steel hollow sections—Part 2: Member behaviour of columns and beams, Journal of Constructional Steel Research. 60, 1319–1332, 2004. https://doi.org/10.1016/j.jcsr.2003.11.007.
- [22] H. Degée, A. Detzel, and U. Kuhlmann, Interaction of global and local buckling in welded RHS compression members, Journal of Constructional Steel Research. 64, 755–765, 2008. https://doi.org/10.1016/j.jcsr.2008.01.032.
- [23] M. Theofanous and L. Gardner, Testing and numerical modelling of lean duplex stainless steel hollow section columns, Engineering Structures. 31, 3047–3058, 2009. https://doi.org/10.1016/j.engstruct.2009.08.004.
- [24] M. Theofanous, T.M. Chan, and L. Gardner, Structural response of stainless steel oval hollow section compression members, Engineering Structures. 31,

- 922–934, 2009. https://doi.org/10.1016/j.engstruct.2008.12.002.
- [25] T.G. Singh and K.D. Singh, Mechanical properties of YSt-310 cold-formed steel hollow sections at elevated temperatures, Journal of Constructional Steel Research. 158, 53–70, 2019. https://doi.org/10.1016/j.jcsr.2019.03.004.
- [26] F. Nishino and L. Tall, Residual stress and local buckling strength of steel columns, Proceedings of the Japan Society of Civil Engineers. 1969, 79–96, 1969. https://doi.org/10.2208/jscej1969.1969.172 79.
- [27] L. Gardner and B. Young, Buckling of ferritic stainless steel members under combined axial compression and bending, Journal of Constructional Steel Research. 117, 35–48, 2016. https://doi.org/10.1016/j.jcsr.2015.10.003.
- [28] J. Chen and T.-M. Chan, Material properties and residual stresses of cold-formed high-strength-steel circular hollow sections, Journal of Constructional Steel Research. 170, 106099, 2020. https://doi.org/10.1016/j.jcsr.2020.106099.
- [29] C. Junbo, C. Tak-Ming, and V.A. Ho, Stub Column Behavior of Cold-Formed High-Strength Steel Circular Hollow Sections under Compression, Journal of Structural Engineering. 146, 04020277, 2020. https://doi.org/10.1061/(ASCE)ST.1943-541X.0002828.
- [30] M. Jia-Lin, C. Tak-Ming, and Y. Ben, Experimental Investigation on Stub-Column Behavior of Cold-Formed High-Strength Steel Tubular Sections, Journal of Structural Engineering. 142, 04015174, 2016. https://doi.org/10.1061/(ASCE)ST.1943-541X.0001456.
- [31] K.J.R. Rasmussen and G.J. Hancock, Plate slenderness limits for high strength steel sections, Journal of Constructional Steel Research. 23, 73–96, 1992. https://doi.org/10.1016/0143-974X(92)90037-F.
- [32] J.B. Dwight and K.E. Moxham, Welded steel plates in compression, The Structural Engineer. 47, 49–66, 1969.
- [33] O. Ikechukwu and İ. Aniekan E., Finite Element Analysis of Tungsten Inert Gas Welding Temperatures on the Stress Profiles of AIS1 1020 Low Carbon Steel Plate, International Journal of Engineering Technologies IJET. 5, 50–58, 2019. https://dergipark.org.tr/tr/pub/ijet/issue/45763/402386.
- [34] F. Uzun and A. Bilge, Total Residual Stress Measurement by Using Ultrasonic Technique, Gazi University Journal of Science. 24, 135–141, 2011. https://dergipark.org.tr/en/pub/gujs/issue/7418/96741.
- [35] D. Rosenthal, Mathematical theory of heat distribution during welding and cutting, Welding Journal. 20, 220–234, 1941.
- [36] N.S. Boulton and H.E.L. Martin, Residual Stresses in Arc-Welded Plates, Proceedings of the Institution of Mechanical Engineers. 133, 295–347, 1936. https://doi.org/10.1243/PIME_PROC_1936_133_017_02.

- [37] Y. Ueda, Elastic, elastic-plastic and plastic buckling of plates with residual stresses. Ph.D. Thesis, Lehigh University, Pennsylvania, United States, 1962.
- [38] Y. Fujita, Built-up column strength. Ph.D. Thesis, Lehigh University, Pennsylvania, United States, 1956.
- [39] L. Tall, The strength of welded built-up columns. Ph.D. Thesis, Lehigh University, Pennsylvania, United States, 1961.
- [40] H. Kihara, Y. Matsuyama, K. Masubuchi, and Y. Ogura, Effect of Welding Sequence on Transverse Shrinkage and Residual Stresses, Journal of Zosen Kiokai. 1956, 123–134, 1956. https://doi.org/10.2534/jjasnaoe1952.1956.99 123.
- [41] M. Yoshiki, Y. Fujita, and T. Kawai, Influence of Residual Stresses on the Buckling of Plates, Journal of Zosen Kiokai. 1960, 187–194, 1960. https://doi.org/10.2534/jjasnaoe1952.1960.107 187.
- [42] Y. Fujita, Influence of Residual Stresses on the Instability Problems, Journal of Zosen Kiokai. 1960, 179–185, 1960. https://doi.org/10.2534/jjasnaoe1952.1960.107_179.
- [43] L. Preserve, A.W. Huber, L.S. Beedle, L.S. And Beedle, and F.E. Laboratory, Residual stress and the compressive strength of steel. Welding Journal, 33 (12), p. 589-s, (December 1954), Reprint No. 96 (54-3), 1954. http://preserve.lehigh.edu/engr-civil-environmental-fritz-lab-reports/1510.
- [44] B.L. S. and T. Lambert, Basic Column Strength, Journal of the Structural Division. 86, 139–173, 1960. https://doi.org/10.1061/JSDEAG.0000539.
- [45] F. Estuar and L. Tall, Experimental investigation of welded built-up columns. The Welding Journal, Vol. 42, p. 164, April 1963, Reprint No. 217 (63-4), 1963.
- [46] Y.-B. Wang, G.-Q. Li, and S.-W. Chen, The assessment of residual stresses in welded high strength steel box sections, Journal of Constructional Steel Research. 76, 93–99, 2012. https://doi.org/10.1016/j.jcsr.2012.03.025.
- [47] M. Khan, A. Paradowska, B. Uy, F. Mashiri, and Z. Tao, Residual stresses in high strength steel welded box sections, Journal of Constructional Steel Research. 116, 55–64, 2016. https://doi.org/10.1016/j.jcsr.2015.08.033.
- [48] prEN 1993-1-14, Eurocode 3: Design of steel structures—Part 1-14: Design assisted by finite element analysis, 2020.
- [49] B. Somodi and B. Kövesdi, Residual stress measurements on welded square box sections using steel grades of S235–S960, Thin-Walled Structures. 123, 142–154, 2018. https://doi.org/10.1016/j.tws.2017.11.028.
- [50] M. Clarin, High strength steel: local buckling and residual stresses. Licentiate dissertation, Luleå tekniska universitet, Luleå, Sweden 2004.
- [51] M. Radwan and B. Kövesdi, Local plate buckling type imperfections for NSS and HSS welded box-section columns, Structures. 34, 2628–2643, 2021. https://doi.org/10.1016/j.istruc.2021.09.011.

- [52] O.-P. Hämäläinen, T. Halme, and T. Björk, Local Buckling of Welded Box Beams Made of Ultrahigh-Strength Steels, Journal of Structural Engineering. 144, 2018. https://doi.org/10.1061/(ASCE)ST.1943-541X.0002049.
- [53] H. Ban, G. Shi, Y. Shi, and Y. Wang, Residual stress of 460MPa high strength steel welded box section: Experimental investigation and modeling, Thin-Walled Structures. 64, 73–82, 2013. https://doi.org/10.1016/j.tws.2012.12.007.
- [54] M. Clarin and O. Lagerqvist, Residual stresses in square hollow sections made of high strength steel, in: Z.Y. Shen, G.Q. Li, S.L. Chan (Eds.), Fourth International Conference on Advances in Steel Structures, Elsevier Science Ltd, Oxford, 2005: pp. 1577–1582. https://doi.org/10.1016/B978-008044637-0/50235-3.
- [55] F. Nishino, Y. Ueda, and L. Tall, Experimental Investigation of the Buckling of Plates with Residual Stresses, in: Test Methods for Compression Members, ASTM International, 100 Barr Harbor Drive, PO Box C700, West Conshohocken, PA 19428-2959, n.d.: pp. 12-12-19. https://doi.org/10.1520/STP43785S.
- [56] K.J.R. Rasmussen and G.J. Hancock, Tests of high strength steel columns, Journal of Constructional Steel Research. 34, 27–52, 1995. https://doi.org/10.1016/0143-974X(95)97296-A.
- [57] M. Seif and B.W. Schafer, Local buckling of structural steel shapes, Journal of Constructional Steel Research. 66, 1232–1247, 2010. https://doi.org/10.1016/j.jcsr.2010.03.015.
- [58] W.D. Kroll, G.P. Fisher, and G.J. Heimerl, Charts for calculation of the critical stress for local instability of columns with I-, Z-, channel, and rectangular-tube section, National Advisory Committee for Aeronautics, 1943.
- [59] M.R. Haidarali and D.A. Nethercot, Finite element modelling of cold-formed steel beams under local buckling or combined local/distortional buckling, Thin-Walled Structures. 49, 1554–1562, 2011. https://doi.org/10.1016/j.tws.2011.08.003.
- [60] R. Siahaan, P. Keerthan, and M. Mahendran, Finite element modeling of rivet fastened rectangular hollow flange channel beams subject to local buckling, Engineering Structures. 126, 311–327, 2016. https://doi.org/10.1016/j.engstruct.2016.07.004.
- [61] M.N. Bin Kamarudin, J.S. Mohamed Ali, A. Aabid, and Y.E. Ibrahim, Buckling Analysis of a Thin-Walled Structure Using Finite Element Method and Design of Experiments, Aerospace. 9, 541, 2022. https://doi.org/10.3390/aerospace9100541.
- [62] E. Ellobody, Nonlinear analysis of cellular steel beams under combined buckling modes, Thin-Walled Structures. 52, 66–79, 2012. https://doi.org/10.1016/j.tws.2011.12.009.
- [63] S.-E. Kim, G. Papazafeiropoulos, V.-H. Truong, P.-C. Nguyen, Z. Kong, N.-T. Duong, V.-T. Pham, and Q.-V. Vu, Finite element simulation of normal – Strength CFDST members with shear connectors under bending

- loading, Engineering Structures. 238, 112011, 2021. https://doi.org/10.1016/j.engstruct.2021.112011.
- [64] A. Mahmoud, S. Torabian, A. Jay, A. Myers, E. Smith, and B. Schafer, Modeling protocols for elastic buckling and collapse analysis of spirally welded circular hollow thin-walled sections, 2015. https://doi.org/10.13140/2.1.4893.7763.
- [65] M. Hosseinpour and Y. Sharifi, Finite element modelling of castellated steel beams under lateral-distortional buckling mode, Structures. 29, 1507–1521, 2021. https://doi.org/10.1016/j.istruc.2020.12.038.
- [66] O.C. Zienkiewicz, R.L. Taylor, and J.Z. Zhu, Chapter 6 Shape Functions, Derivatives, and Integration, in: O.C. Zienkiewicz, R.L. Taylor, J.Z. Zhu (Eds.), The Finite Element Method: Its Basis and Fundamentals (Seventh Edition), Butterworth-Heinemann, Oxford, 2013: pp. 151–209. https://doi.org/10.1016/B978-1-85617-633-0.00006-X.
- [67] P. Wysmulski, The analysis of buckling and post buckling in the compressed composite columns, Archives of Materials Science and Engineering. 85, 35–41, 2017. https://doi.org/10.5604/01.3001.0010.1556.
- [68] Y. Wu, S. Fan, L. Du, and Q. Wu, Research on distortional buckling capacity of stainless steel lipped C-section beams, Thin-Walled Structures. 169, 108453, 2021. https://doi.org/10.1016/j.tws.2021.108453.
- [69] E. Ellobody, Buckling analysis of high strength stainless steel stiffened and unstiffened slender hollow section columns, Journal of Constructional Steel Research. 63, 145–155, 2007. https://doi.org/10.1016/j.jcsr.2006.04.007.
- [70] M. Liu, L. Zhang, P. Wang, and Y. Chang, Buckling behaviors of section aluminum alloy columns under

- axial compression, Engineering Structures. 95, 127–137, 2015. https://doi.org/10.1016/j.engstruct.2015.03.064.
- [71] M. Longshithung Patton and K. Darunkumar Singh, Buckling of fixed-ended lean duplex stainless steel hollow columns of square, L-, T-, and +-shaped sections under pure axial compression—a finite element study, Thin-Walled Structures. 63, 106–116, 2013. https://doi.org/10.1016/j.tws.2012.09.003.
- [72] S.S. Kim, J.Y. Kim, and T.S. Kim, Finite element Analysis on Buckling Strength of Stainless Steel Circular Hollow Section Columns Under Concentric Axial Compression, International Journal of Steel Structures. 20, 1831–1848, 2020. https://doi.org/10.1007/s13296-020-00366-w.
- [73] P. Sarir, H. Jiang, P.G. Asteris, A. Formisano, and D.J. Armaghani, Iterative Finite Element Analysis of Concrete-Filled Steel Tube Columns Subjected to Axial Compression, Buildings. 12, 2022. https://doi.org/10.3390/buildings12122071.
- [74] B. Paul, K. Roy, J.B.P. Lim, Z. Fang, K. McCollum, and D. Bell, Moment-capacity of bolted side-plates for apex joint of nested tapered box beam portal frames, Journal of Building Engineering. 76, 107011, 2023. https://doi.org/10.1016/j.jobe.2023.107011.
- [75] N. Rathinam and B. Prabu, Static buckling analysis of thin cylindrical shell with centrally located dent under uniform lateral pressure, International Journal of Steel Structures. 13, 509–518, 2013. https://doi.org/10.1007/s13296-013-3010-5.
- [76] B.N. Parlett and B. Nour-Omid, Towards a black box Lanczos program, Computer Physics Communications.
 53, 169–179, 1989. https://doi.org/10.1016/0010-4655(89)90158-6.

